Heliyon 10 (2024) e38306

Contents lists available at ScienceDirect

Heliyon

journal homepage: www.cell.com/heliyon

Research article

Oxidative stress gene signature construction to identify subtypes and prognosis of patients with lung adenocarcinoma

Lan Li [a,b,1], Rujia Qin [c,1], Xuefeng Wang [d,1], Ke Cao [a,1], Fei Lu [a], Zhengting Chen [a], Jingyan Gao [a], Linbo Qiu [a], Sisong Shu [a], Han Lu [a], Li Chang [a,**], Wenhui Li [a,*]

[a] Department of Radiation Oncology, The Third Affiliated Hospital of Kunming Medical University/Yunnan Cancer Hospital/Peking University Cancer Hospital Yunnan, Kunming 650118, Yunnan, China
[b] Key Laboratory of Lung Cancer Research of Yunnan Province, The Third Affiliated Hospital of Kunming Medical University/Yunnan Cancer Center, Kunming 650118, Yunnan, China
[c] Department of oncology, Northern Jiangsu People's Hospital, Yangzhou 225000, PR China
[d] Department of Hepatobiliary Surgery, Xiantao First People's Hospital, Xiantao 433000, Hubei, China

ARTICLE INFO

Keywords:
Lung adenocarcinoma
Differentially expressed genes
Oxidative stress response-related genes
Prognosis
Drug sensitivity

ABSTRACT

Background: Although oxidative stress and malignancies are intimately connected, it is unknown how lung adenocarcinoma (LUAD) is affected by oxidative stress response-related genes (OSRGs). Our goal in this work was to create a genetic signature based on OSRGs that might both predict prognosis and hint to potential treatment options for LUAD.
Methods: Clinicopathological and transcriptome information on LUAD patients was obtained from the Cancer Genome Atlas (TCGA) and Gene Expression Omnibus (GEO) databases. A model for predicting risk was created using LASSO regression. The TCGA, GSE72094, and GSE41271 cohorts all demonstrated the risk model's prediction ability. Immune cell infiltration was measured using the CIBERSORT method, and the TIDE platform was implemented to evaluate the therapeutic efficacy of immune checkpoint inhibition (ICI). Chemotherapy sensitivity was predicted using drug activity data by the Genomics of Drug Sensitivity. An investigation into gene expression was conducted using qRT-PCR. CCK-8 and transwell assays were employed to look into how DKK1 affected the migration and proliferation of LUAD cells.
Results: A gene signature consisting of *ANLN*, *FAM83A*, *DKK1*, *LOXL2*, *RHOV*, *IGFBP1*, *CCR2*, *GNG7*, and *C11orf16* was efficiently determined and used to calculate a patient-specific risk score, this functioned as a stand-alone biomarker for prediction. Correlations were found between risk scores and immune cell infiltration frequency, ICI therapy response rate, estimated chemotherapeutic drug susceptibility and autophagy-related genes.Furthermore, DKK1 knockdown reduced the ability of LUAD cells to multiply and migrate.
Conclusion: Our thorough transcriptome study of OSRGs generated a biological framework effective in forecasting outcome and responsiveness to therapy in LUAD patients.

* Corresponding author. Department of Radiation Oncology, The Third Affiliated Hospital of Kunming Medical University/Yunnan Cancer Hospital, 519 Kunzhou Road, Kunming 650118, Yunnan, China.
** Corresponding author.
E-mail addresses: changli1981@126.com (L. Chang), wenhuili64@yeah.net (W. Li).
[1] Lan Li, Rujia Qin, Xiao Jiang, and Ke Cao should be considered joint first authors.

https://doi.org/10.1016/j.heliyon.2024.e38306
Received 21 August 2023; Received in revised form 8 September 2024; Accepted 22 September 2024
Available online 24 September 2024

1. Background

Lung cancer has the most severe effects of all the many forms of cancer [1,2]. As lung cancer is generally diagnosed and treated when it has reached an advanced stage, it frequently spreads quickly and has a high risk of recur. About 70 % of non-small cell lung malignancies are caused by lung adenocarcinoma (LUAD), which has a negative outcome [3,4]. Thus, developing a novel, sensitive, and trustworthy forecasting method to precisely forecast the prognosis of LUAD patients and steer logical treatment plans is a potential path.

A major contributing element to the emergence and progression of tumors is oxidative stress.The buildup of reactive oxygen species (ROS) is the source of cellular oxidative stress. There have been many studies showing that many cancers [5–14], such as lung, liver, breast, prostate, and other cancers, are all related to oxidative stress, as well as other benign diseases [15]. Targeting oxidative stress can promote or inhibit tumour growth; therefore, controlling tumour cells' redox homeostasis may improve the tumors' therapeutic outcome. Oxidative stress affects the prognosis of various tumors with anti-tumour or pro-tumour regulation by its associated genes. Bioinformatics and other substantial data analysis techniques can be used to identify novel treatment targets and evaluate the heterogeneity of oxidative stress in cancer.

Hence, within this research, we built a predictive model using nine oxidative stress-related genes (ORGs) that influence survival in LUAD and verified its predictive efficacy in TCGA and GEO cohorts, apart from evaluating oxidative stress prognostic genes about genomic mutations, immunological profiles, sensitivity to drugs and autophagy-related genes. Ultimately, nine genes that display an oxidative stress signature in the LUAD cell line were found using quantitative real-time PCR tests. Moreover, the impact of DKK1 on LUAD cells' proliferation and migration ability was verified. This model will guide prognostic prediction and efficacy monitoring in individualised clinical treatment. **Fig. 1** showed the overall framework of this research.

2. Materials and Methods

2.1. Datasets

The Cancer Genome Atlas (TCGA) and the GEO database were used to collect detailed clinical data and gene expression from individuals with LUAD. The LUAD information were selected based on the clinical information. The GEO database provided the gene expression matrix for GSE72094. Illumina probe annotation files were obtained from GPL15048. Here is how the TCGA-LUAD and GSE72094 data were handled: (1) Gene symbol conversion of the probe or ensemble ID; (2) Removal of probes pertaining to multiple genes; (3) When there are several probes or ensemble IDs that belong to a single Gene Symbol, by applying the mean value of the Gene Symbol, the expression value of the gene was calculated. The Gene's median value Symbol is interpreted as the gene's expression value. As TCGA and GEO are publicly accessible databases, ethical assessment was not required. Processed TCGA-LUAD data were from 487 cancer and 81 para-cancer tissue samples, while GSE72094 data was from 442 cancer tissue samples. The Molecular Signatures Database (v7.5.1) identified a total of 436 OSRGs.

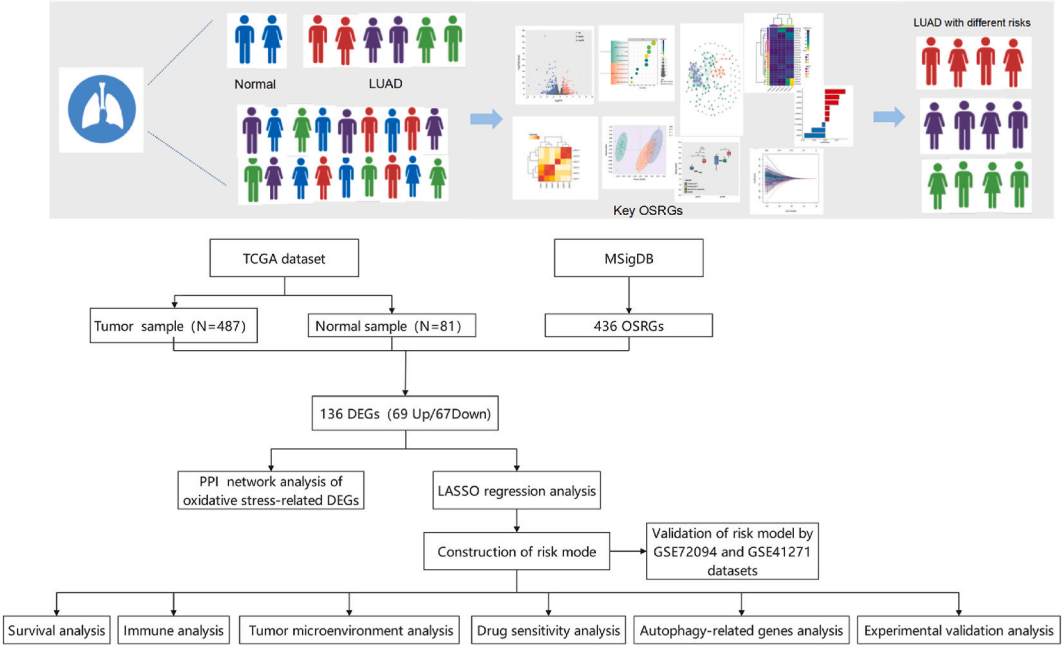

Fig. 1. The study design was shown basically in the flow graph.

2.2. Network analysis of protein-protein interactions (PPIs)

An internet resource known as STRING that includes data on real and potential protein interactions was used to analyze the PPI network. A PPI network was utilized to assign OSRGs, and a threshold value of >0.4 for confidence scores was developed.

2.3. Consensus clustering

Using the "ConsensusClusterPlus" software program, we grouped LUAD patients into several subtypes in order to examine the biological roles of OSRGs in LUAD. The "ConsensusClusterPlus" program uses the Euclidean metric distance computation and the k-means clustering algorithm with 1000 iterations and an 80 % reprocessing rate.The Kaplan-Meier (KM) technique was employed to assess survival rates and compare results across various subgroups.

2.4. Developing and verifying the prognostic OSRG signature

To locate DEGs, the 'limma' package was utilized with the following criteria applied: |log 2 fold-change (FC)| > 0.5, FDR <0.05. DEGs and OSRGs were investigated using one-way Cox regression analysis. Then, multicollinearity was decreased using LASSO Cox regression analysis. In the regression analysis, the dependent variable is the patients' overall survival and status within the TCGA cohort, whereas the independent variable is the genes' standardized expression networks. Gene expression levels and the associated regression coefficients were used to compute patient risk ratings. The model was built with the cv.glmnet function in the R package 'glmnet' for k-fold cross-validation with default parameters, using 5-fold cross-validation, and risk ratings determined using the method for every patient. The "survminer" software was used to investigate the difference in OS survival between high-risk and low-risk groups, which were classified according on the median risk score. KM curves were plotted using the R software package "survminer." Finally, validation cohort calculated risk scores using the same formula.

2.5. Analysis of functional enrichment

To evaluate the likely biological functions of DEGs among LUAD oxidative stress subtypes, pathway analysis from the Kyoto Encyclopedia of Genes and Genomes and gene ontology functional enrichment analysis were performed using the 'clusterProfiler' program.

2.6. Assessment of immune cell infiltration

LUAD tumor immune microenvironment (TIME) penetration percentage of immune cells was determined by single sample gene set enrichment analysis (ssGSEA). Based on research by Charoentong (PMID: 28052254), which identified genes enriched for many human immune cell categories, gene sets were identified for each TIME-infiltrating immune cell type.

2.7. Chemotherapy response estimation

The "calcPhenotype" method of the R package "oncoPredict," which is built on the GDSC (https://www.cancerrxgene.org/) cancer genomics drug sensitivity database, was used to determine the drug IC50 measurements for every sample in the training set. Calculating the Spearman correlation values between the risk score and drug IC50 values, as well as analyzing the variations between small-molecule drug IC50 values in the high- and low-risk score groups, allowed us to examine the relationship between small-molecule drug sensitivity and risk score.

2.8. Prediction of immune checkpoint inhibition therapy

Using the R package version 0.2 (https://CRAN.R-project.org/package=oncoPredict), the tumor immune dysfunction and exclusion (TIDE) approach was employed for estimating immunotherapy response and TIDE values obtained from TCGA-LUAD expression data.

2.9. Cell culture and quantitative real-time PCR (qRT-PCR)

The Institute of Biochemistry and Cell Biology (Shanghai, PR China) supplied the B2B, A549, H1734, H1650, and H1299 human lung cancer cell lines. The Xuanwei LUAD XWLC-05 (Xuanwei Lung Cancer-05) cell line was donated by the Laboratory of Lung Cancer, Yunnan Cancer Hospital. Using the TRIzol reagent, total RNA samples were extracted from each cell line, and the SYBR Green Master Mix kit was implemented to do reverse transcription.

2.10. Analytical statistics

R 4.1.2 was employed to do the statistical analysis. The KM approach was performed to generate survival curves, and the log-rank test served to evaluate group differences. The 1-, 3-, and 5-year total OS prediction efficiency of the risk model was measured utilizing

ROC curves. At $p < 0.05$, the criterion for statistical significance was established. To determine DEGs between LUAD tissue and LUAD paracancer specimens, the R "limma" package was applied. Volcano and heat maps created using R packages 'ggplot 2' and 'ComplexHeatmap'.

3. Results

3.1. Differential expression of OSRGs in LUAD

Based on TCGA-LUAD data from 487 cancer and 81 paraneoplastic tissue samples, With FDR <0.05 as the cutoff, $|\log_2 FC| > 0.5$, 136 of 436 OSRGs were considerably differentially showed between LUAD and normal tissue samples, indicating that OSRGs may participate a crucial role in LUAD growth. The 136 critical oxidative stress genes included 67 genes were down-regulated and 69 were up-regulated. Volcano and heat maps showing OSRG expression in LUAD are shown in Fig. 2A and B.

OSRGs were also differentially expressed according to clinical features in TCGA-LUAD data. *NDUFS8* and *EZH2* were differentially expressed among patient age subgroups (<60 and ≥ 60 years), while *FANCD2* and *RGS14* expression differed according to clinical stage (stage I, stage IV). In contrast to LUAD patients who were not treated with radiation treatment, radiation treatment patients had higher expression levels of the *EZH2*, *FANCD2*, *GSS*, *NDUFS8*, *NONO*, and *PRDX2* genes. Further, *HGF* and *MSRB3* expression levels were higher in the subgroup of LUAD patients with an EGFR mutation than in those without. In addition, *HGF* and *MSRB3* levels varied considerably by ethnicity, whereas those of *EZH2*, *FANCD4*, *MSRB3*, and *RGSJ4* substantially differed by sex (Fig. 2C–H).

Using the STRING database, we built a PPI network via the 136 that differ in OSRGs, to examine their interactions within LUAD. It was clear from the findings that CASP3, IL6, CAT, JUN, HIFIA, HMOXI, TXN, TLR4, PTGS2, FOS, GSR, MMP9, LRRK2, and FOXO3 had a high levels of network connection, and we hypothesized that these genes could be crucial for LUAD. (Fig. 2I). Furthermore, we examined relationships among OSRGs and discovered that levels of *GCLC* were positively correlated with those of *GCLM* and *AIFM2*, while *AIFM2* levels were in direct opposition to those of *BTK* and *FUT8*. These data indicate that there may be mutual regulation among OSRGs (Fig. 2J).

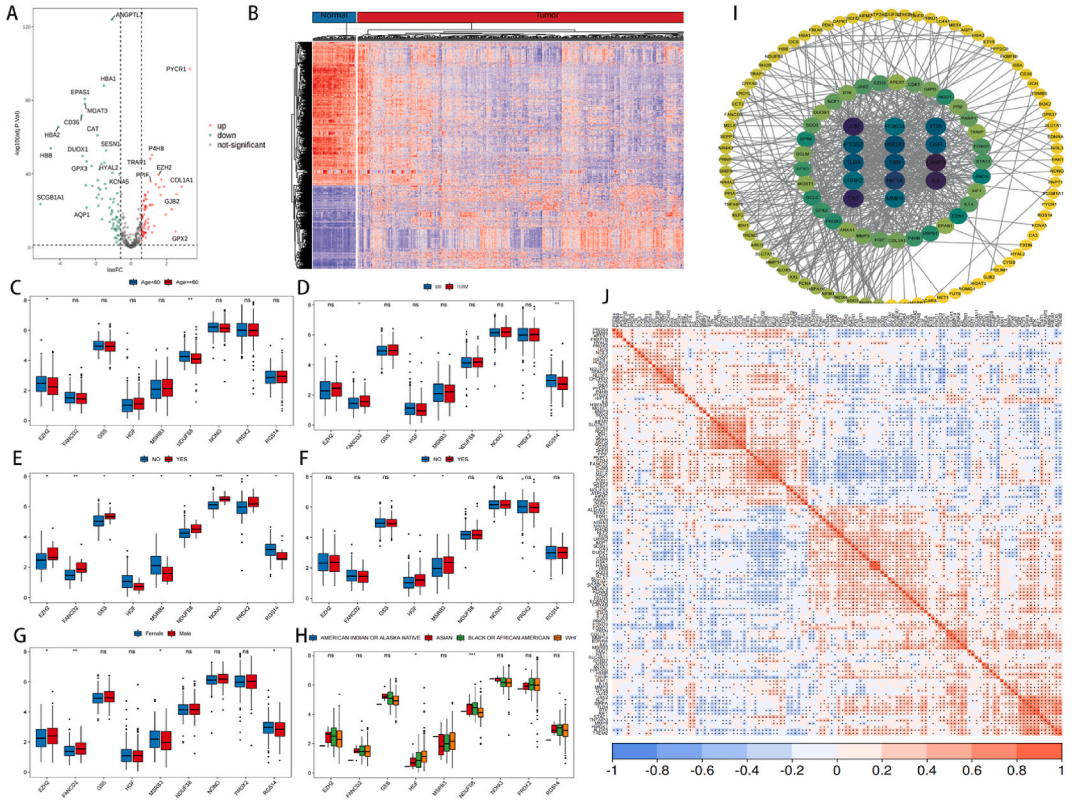

Fig. 2. Differential expression of OSRGs in LUAD. (A) Map of volcanoes. **(B)** Gene expression map at different levels. Depending on the characteristics of the patient, OSRGs expression varied, including: **(C)** age, **(D)** clinical stage, **(E)** radiotherapy, **(F)** EGFR mutation, **(G)** sex, and **(H)** ethnicity. **(I)** Network diagram of OSRGs with variable expression. **(J)** OSRGs with variably expressed correlation heat maps.

3.2. Identification of OSRG molecular subtypes and differences in clinical features among subtypes

In accordance with the expression characteristics of the 436 OSRGs that have been established, TCGA-LUAD tumor samples were submitted to clustering analysis, generating almost flat CDF curves (range, 0.1–0.9) at k = 3. The "inflection point method" was subsequently employed to investigate the relative change in the region below the CDF curve as the number of clusters expanded in order to determine the optimal number of clusters, and three classes selected as the final number of clusters (Figs. 3A and 2B), enabling the separation of materials into three subtypes (Fig. 3C), as follows: Cluster1 (N = 180), Cluster2 (N = 188), and Cluster 3 (N = 119). To reduce the dimensionality of the data, the uniform manifold approximation and projection (UMAP) technique was implemented, and the results indicated that the samples were accurately classified into three categories according to the OSRGs (Fig. 3D).

Next, based on the three OSRG subtypes, we assessed the variations in their clinical characteristics, including age, gender, race, stage, receipt of radiation therapy, and EGFR mutations, and the findings demonstrated that the three subgroups exhibited a substantial difference in terms of gender and clinical stage (Fig. 3E). In TCGA-LUAD cohort data, prognostic KM survival curves for the three subtypes varied considerably ($p < 0.05$). Relative to patients in Cluster2 and Cluster 3, those in Cluster1 had excellent prognosis and the longest overall OS, disease-free interval, and disease-specific survival (Fig. 3F–H). In order to more thoroughly examine the connection between the three forms of oxidative stress and immunological state, we contrasted the tumor purity, stromal, immunological, and ESTIMATE scores among the three subtypes using the 'ESTIMATE' package and found that all these parameters differed among them ($p < 2.21e-16$). The calculated score is a combination of immune and stromal factors. The makeup of stromal and immune

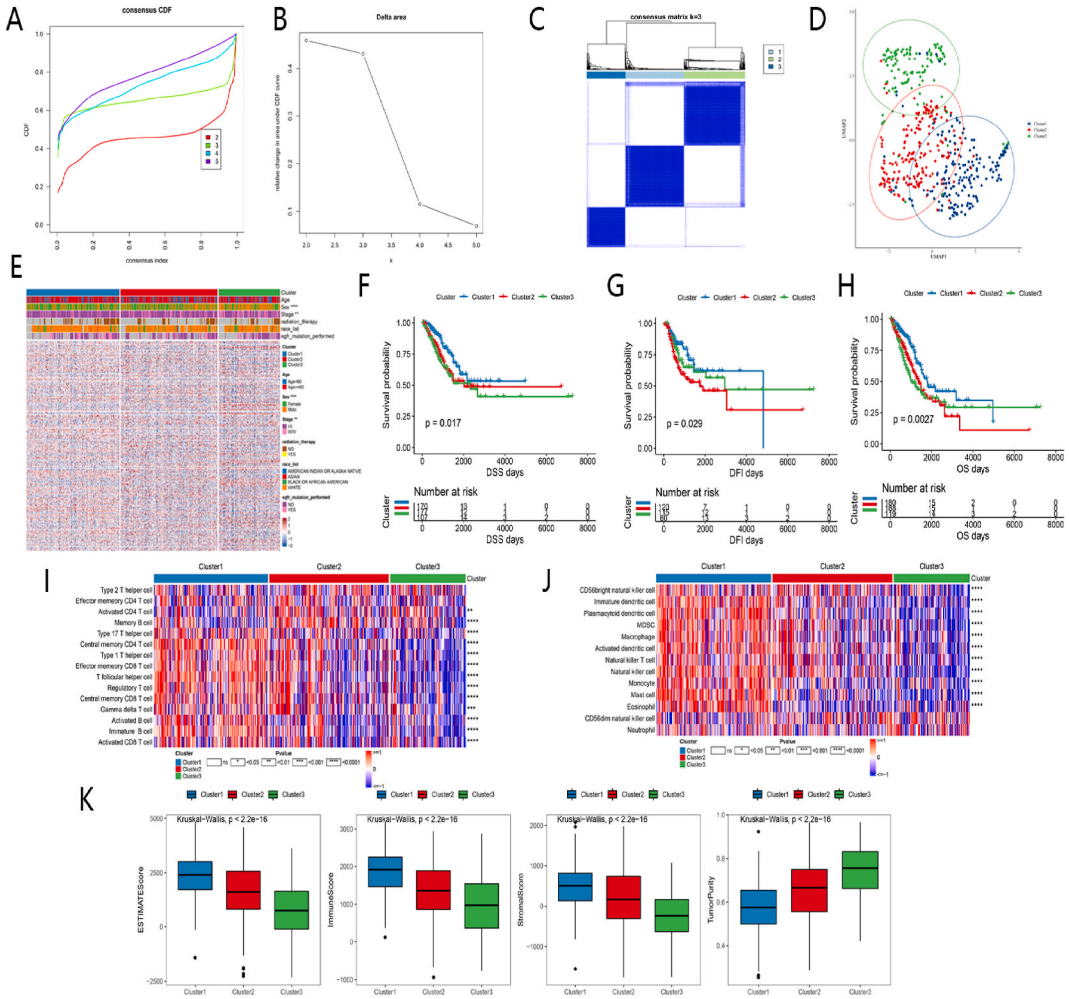

Fig. 3. Molecular subtype identification of OSRGs and differences in clinical features among patients in OSRG subtypes. (**A**) CDF curve distribution of consistent clustering. (**B**) Clustering-consistent CDF curve. (**C**) Clustering results at classification number k = 3. (**D**) UMAP clustering results of 436 OSRGs. (**E**) A heat map showing how clinical indications are distributed throughout the three kinds. Survival curves of the three OSRG subtypes: (**F**) Disease-specific survival, (**G**) Disease-free interval, (**H**) Overall survival. (**I**) Inter-subtype immune infiltration microenvironment. Heat map showing the three OSRG subtypes' respective ADAPTIVE immune cell infiltration scores. (**J**) The three OSRG subtypes' INNATE immune cell infiltration score is shown in heat map. (**K**) Box line plot of ESTIMATE scores in the three OSRG subtypes.

cells was evaluated by calculating stromal and immunological scores, based on which tumour purity was further inferred. It was noteworthy that patients were more likely to have greater tumor purity when they had higher OS ratings. In Cluster 1, higher stromal and immune scores are associated with lower tumour purity and better prognosis (Fig. 3K). In order to enhance the comprehension of the differences among the three subcategories of TIME, and to find the immunological scores connected to the various molecular subtypes, we relied on the ssGSEA program.Our analysis showed that infiltration scores for ADAPTIVE and INNATE immune cells differed significantly among three subtypes. The findings demonstrated that the three subtypes differed in terms of different infiltrating immune cells, including activated CD4 T cell ($p < 0.01$), memory B cell ($p < 0.0001$), type 17 T helper cell ($p < 0.0001$), central memory CD4 T cell ($p < 0.0001$), type 1 T helper cell ($p < 0.0001$), effector memory CD8 T cell ($p < 0.0001$), T follicular helper cell ($p < 0.0001$), regulatory T cells ($p < 0.0001$), central memory CD8 T cell ($p < 0.0001$), gamma delta T cells ($p < 0.001$), activated B cell ($p < 0.0001$), immature B cell ($p < 0.0001$), activated CD8 cell ($p < 0.0001$), CD56bright nature killer cell ($p < 0.0001$), immature dendritic cell ($p < 0.0001$), MDSC ($p < 0.0001$), macrophage ($p < 0.0001$) etc. Infiltration scores of innate and adaptive immune cells were best in Cluster 1, portending a good prognosis (Fig. 3I and J). These findings indicate that OSRGs in LUAD could be immune-related.

3.3. OSRG signature construction in LUAD

Between the three OSRG subtypes, an study of univariate Cox regression was performed on 1173 DEGs. Of these DEGs, 485 were linked to a patient's prognosis ($P < 0.05$). According to these 485 genes involved in prognosis, LASSO Cox analysis was further employed to remove redundant genes and screen out 9 core prognostic genes (Fig. 4A–C); *ANLN ($P < 0.001$)*, *FAM83A ($P = 0.0019$)*, *DKK1 ($P < 0.001$)*, *LOXL2 ($P < 0.001$)*, *RHOV ($P = 0.0022$)*, and *IGFBP1 ($P = 0.0044$)* were linked to a poor outcome, whereas *CCR2 ($P < 0.001$)*, *GNG7 ($P < 0.001$)*, and *C11orf16 ($P = 0.001$)* were connected to favorable patient outcomes (Fig. 4D–L). When lambda = 0.0716, a total of 9 genes were filtered for further investigation. A risk-scoring model was created by utilizing the LASSO regression coefficient that forecasts patient survival by ranking the expression of these nine genes. Score = ANLN * 0.061 + DKK1 * 0.088 + LOXL2 * 0.058 + FAM83A * 0.017 + RHOV * 0.019 + IGFBP1 * 0.019 - GNG7 * 0.091 - CCR2 * 0.059 - C11orf16 * 0.013.

Signature = $\sum Coefi * Expri$ (expr represents gene expression level and coef represents LASSO regression coefficient)

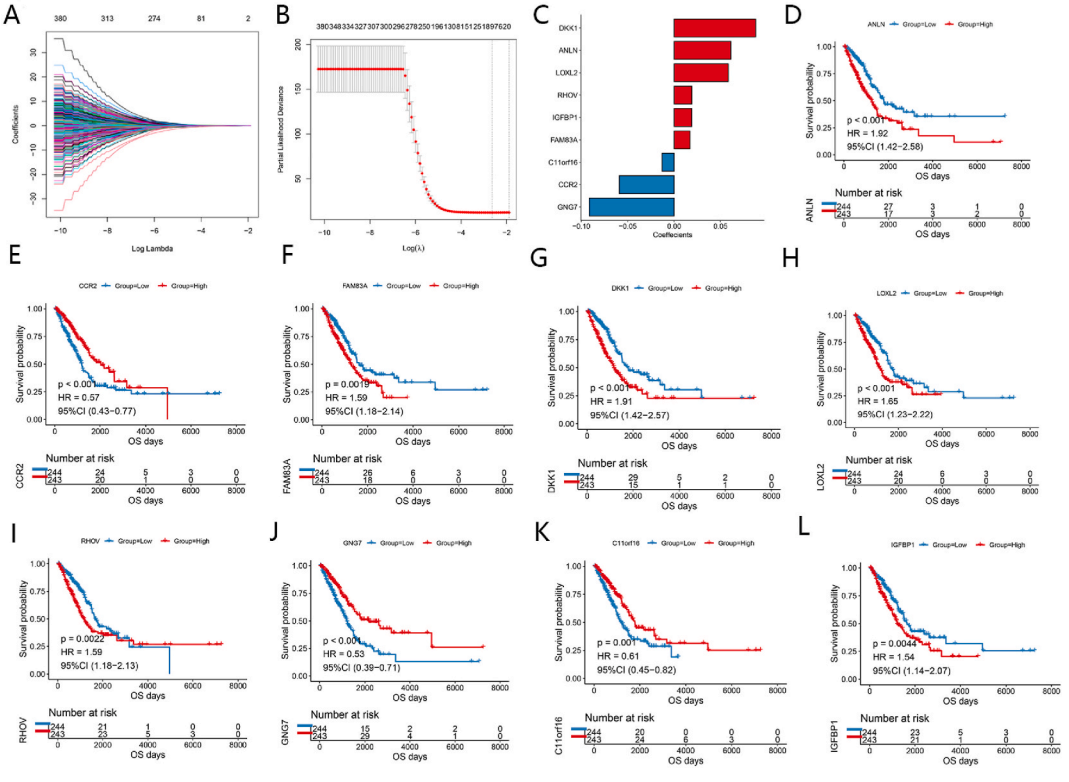

Fig. 4. OSRG signature construction in LUAD. (**A**) The variable that is independent In LASSO regressions, the horizontal coordinate represents lambda's logarithm, and the vertical coordinate represents its coefficient. (**B**) In LASSO analysis, the confidence interval is calculated for each Lambda value. (**C**) Important prognostic gene values according to LASSO regression coefficients. (**D–L**) Survival curves for nine key prognostic genes.

3.4. The OSRG signature can predict patient prognosis

Using our risk score model, we gave each cancer patient sample a risk score. The median score of LUAD samples was applied to divide them into high and low risk categories. ROC curve analysis was performed to evaluate the model's predictive power. In training set TCGA-LUAD data, the prognosis was worse for high-risk cohort ($P < 0.001$) (Fig. 5A), and expected AUC values of data sets at 1, 3, and 5 years were 0.760, 0.714, and 0.660, correspondingly (Fig. 5B), indicating the outstanding predictive value of the model. In the validation set GSE72094, furthermore, the high-risk group's results were poorer ($P < 0.001$) (Fig. 5F), and a predicted AUC values at 1, 3, and 5 years were, in that order, 0.69, 0.68, and 0.651 (Fig. 5G), indicating positive validation of the model. We added the validation set GSE41271 data from 275 cancer tissue samples. In line with the findings from the prior dataset, the high-risk group in the validation set GSE41271 also had an adverse result ($P < 0.001$) (Fig. 5K), with projected AUC values of 0.689, 0.685, and 0.666 for the samples at 1, 3, and 5 years, each (Fig. 4L), indicating positive validation of the model. The risk model was implemented to determine how high- and low-risk populations were distributed throughout the validation and training sets (Fig. 5C, H, 5M). In general, compared to low-risk groups, high-risk ones had shorter OS durations. (Fig. 5D, I, 5N). Further, distinct variations were observed in the distribution of genes that function in the construction of models between the populations at high risk and low risk. As expected from the previously discovered prognostic genes, there was greater expression of ANLN, FAM83A, DKK1, LOXL2, RHOV, and IGFBP1 in the group at high risk as opposed to the group at low risk (Fig. 5E, J, 5O).

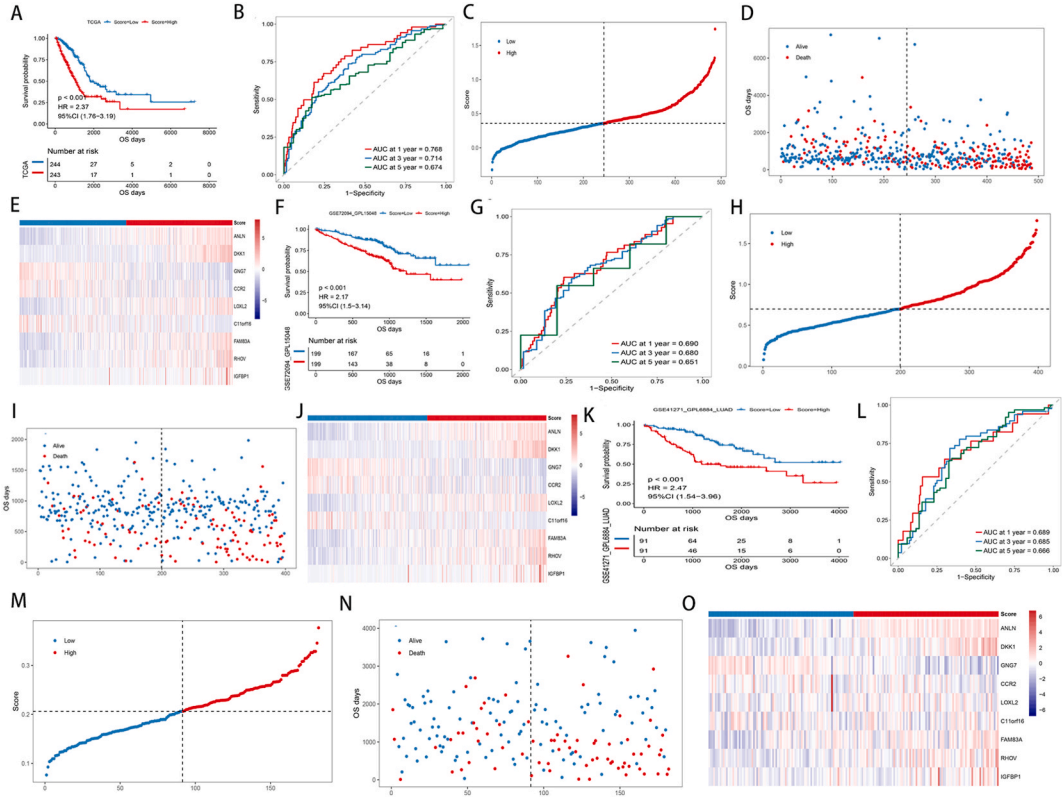

Fig. 5. Model prediction performance is assessed using the GSE validation dataset and the TCGA training dataset. (**A**) Patients' prognoses in the TCGA training dataset's high- and low-risk categories. (**B**) AUC values for samples in the TCGA training dataset at1,3, and 5 years. (**C**) Proportion of high- and low-risk populations identified by the risk model in TCGA training dataset. (**D**) Survival time of high-risk and low-risk populations distinguished by the risk model in TCGA training dataset. (**E**) Variations in the gene distribution that the risk model in the TCGA training dataset used to identify the high-risk and low-risk groups. **Evaluation of model prediction performance in the validation dataset (GSE72094)**. (**F**) Patients' prognoses in the validation dataset's high-risk and low-risk categories (GSE72094). (**G**) AUC values in the validation dataset (GSE72094) for samples at 1, 3, and 5 years. (**H**) Proportion of high-risk and low-risk populations distinguished by the risk model in validation dataset (GSE72094). (**I**) Survival time of high-risk and low-risk populations distinguished by the risk model in validation dataset (GSE72094). (**J**) Variations in the distribution of genes used to build the models across the populations classified as high- and low-riskin line with what is supposedly the validation dataset's risk model (GSE72094). (**K**) Patients' prognoses in the validation dataset's high-risk and low-risk categories (GSE41271). (**L**) AUC values for samples in the validation dataset at1,3, and 5 years (GSE41271). (**M**) Proportion of high-risk and low-risk populations distinguished by the risk model in validation dataset (GSE41271). (**N**) The validation dataset (GSE41271) shows the survival time of populations classified as high-risk and low-risk given the risk model. (**O**) Variations in the gene distribution that were used to build the models between the populations classified as high- and low-risk as stated by the validation dataset's risk model (GSE41271).

3.5. LUAD patients' independent prognostic factor: a signature verified by univariate and multivariate Cox regression analysis

The clinical data (tumor stage, gender, age, etc.) and prognostic model risk scores of the patients were subjected to univariate and multivariate Cox regression analysis. It carried out in the TCGA-LUAD training set indicated that survival in patients with LUAD was correlated with prognostic model risk scores and stage ($p < 0.001$, $HR > 1$) (Fig. 6A and B). Similarly, in the validation datasets GSE72094 and GSE41271, univariate and multivariate Cox regression analyses demonstrated that prognostic modeling risk scores and stage may be employed as standalone prognostic variables predicting the likelihood of survival of patients with LUAD. (Fig. 6C, D, 6E, 6F). We then looked at correlation within model risk scores and clinical characteristic subgroups. Significant differences in model risk scores were found in age ($P < 0.05$), gender ($P < 0.01$), and clinical stage ($P < 0.05$) (Fig. 6G–L). Patients with malignancies in stages III and IV had higher scores than those in stages I and II, showing that individuals with advanced illness have a poorer prognosis. Male patients had higher scores than females, and patients younger than 60 had higher scores, with higher scores associated with a worse prognosis.

3.6. OSRG signature-related molecular and tumor microenvironment features

Further investigation was conducted into correlation within the mutational landscape and risk score by SNV and CNV mutation data of TCGA-LUAD patients. The samples were divided into two categories: high-risk and low-risk, pursuant to the median risk score. A waterfall plot displayed extensive mutation information of the various genes in every sample collected. The top 10 mutated genes were presented in figure. According to SNV alteration data, the frequencies of mutations of TP53, CSMD3, AHNAK, SMARCA4, COL22A1, TEX15, NCOR2, DOCK4, MAGI2, and SLX4 in the two categories were either reasonably high. Moreover, we created low-risk and high-risk score subgroups' amplified or removed CNV on-plots. The top 10 genes of AGBL2, AUTS2, CAMP, CDC25A, EMB, FNBP4, HCN1, NINL, RBFOX1, and UCN2 in high-risk group were comparatively high, based on CNV mutation data. We discovered that the high-risk group experienced more mutation rates in comparison with low-risk group. Immunotherapy perhaps greater successful since the SNV and CNV in high-risk group shown a significant disparity in low-risk group.Tumor HALLMARK enrichment scores were computed and group differences were assessed using ssGSEA and TCGA-LUAD expression data. The following major variations were found in the HALLMARK pathway after analyzing the variation in groups with high and low risk scores: HALLMARK EPITHELIAL MESENCHYMAL TRANSACTION, HALLMARK HYPOXIA, HALLMARK APICAL SURFACE, HALLMARK MYOGENESIS, HALLMARK DNA REPAIR, and HALLMARK FAITY ACID METABOLISM etc. The relevance of these pathways to oxidative stress may provide direction for targeting oxidative stress (Fig. 7D). Additionally, the ImmuneScore, StromalScore, and EstimateScore were computed using the ESTIMATE algorithm, and low-risk group was found to have higher test results, suggesting better immune activation (Fig. 7E and F). Further, CIBERSORT analysis was employed for computing immune cell infiltration and revealed that the immune trend was in line

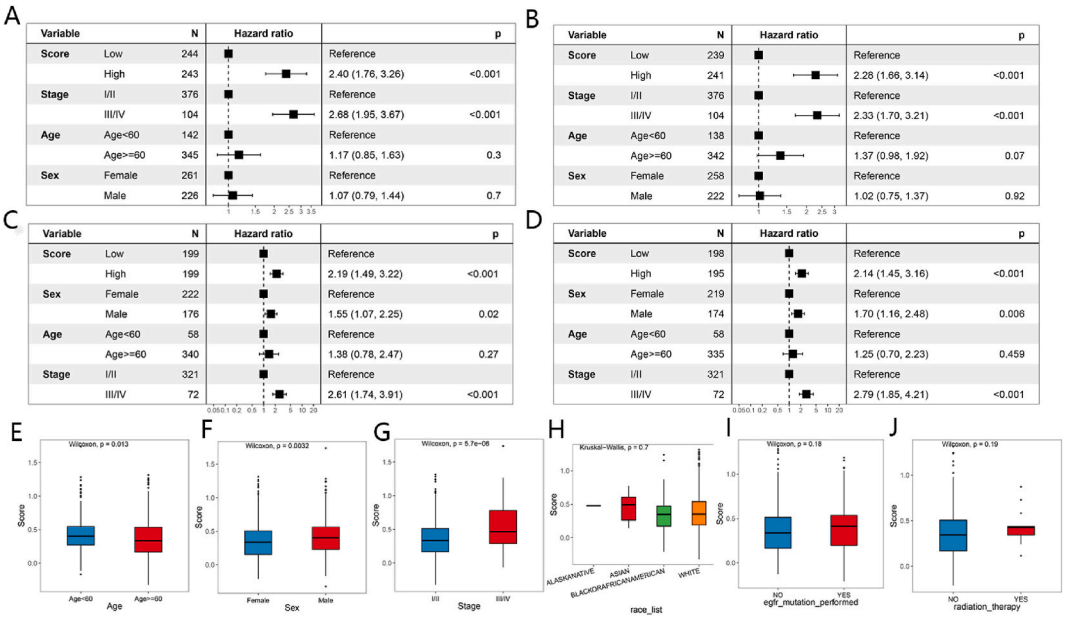

Fig. 6. Cox regression examination of the relationships between clinical features and model risk scores in the GSE validation and TCGA training datasets. (**A**) Cox regression analysis using a single component in the training dataset for TCGA. (**B**) Cox regression analysis with multi-factor in the training dataset of TCGA. Cox regression analysis of clinical characteristics associations with model risk score in GSE72094 validation dataset. (C, E) Single-factor Cox regression analysis in GSE72094 and GSE41271 validation dataset. (D, F) Multi-factor Cox regression analysis in GSE72094 and GSE41271 validation dataset. Differences in model risk scores according to clinical characteristic subgroups, including (**G**) age, (**H**) sex, (**I**) tumor stage, (**J**) ethnicity, (**K**) EGFR mutation, and (**L**) radiotherapy.

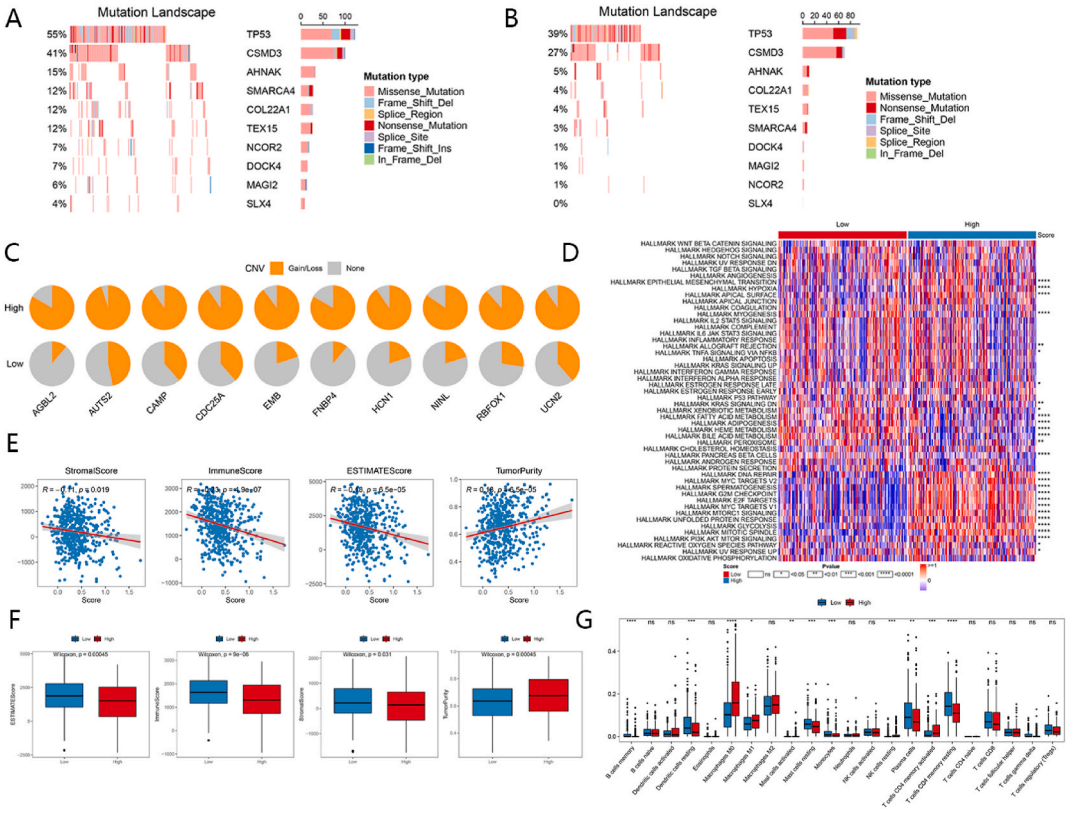

Fig. 7. OSRG signature-related molecular features and tumor microenvironment. (**A**) The waterfall graphic displayed the top 10 genes in the high risk score group's LUAD that had the greatest frequency of mutations. (**B**) The waterfall graphic displayed the top 10 genes in low risk score group's LUAD that had the greatest frequency of mutations. (**C**) The top 10 genes of amplificated or deleted CNV distribution diagram of groups with high and low risk score groups. (**D**) Variations in the HALLMARK routes in the groups with high and low risk scores. (**E, F**) Comparison of ESTIMATE immune infiltration rates of various subgroups. (**G**) The distribution of 22 immune cells across the two risk categories is displayed in CIBERSORT immune cell infiltration scores box plot.

with the ESTIMATE analysis's findings. Additionally, low-risk group outperformed the high-risk group in terms of immune cell infiltration according to CIBERSORT analysis. These included resting memory CD4 T cells ($p < 0.0001$), resting dendritic cells ($p < 0.001$), resting memory B cells ($p < 0.0001$), monocytes ($p < 0.001$), plasma cells ($p < 0.01$), and resting mast cells ($p < 0.001$). Activated memory $CD4^{+}$ T cells ($p < 0.001$), activated mast cells ($p < 0.01$), M0 macrophages ($p < 0.0001$), M1 macrophages ($p < 0.05$), and resting NC cells ($p < 0.001$) were significantly more elevated for individuals with high-risk scores. Then, in two groups of activated dendritic cells, eosinophils, naïve B cells, etc., there was definitely no significance (Fig. 7G). The low-risk group had the strongest innate and adaptive immune cell infiltration ratings, indicating a favorable prognosis.

3.7. Comparison of drug response and autophagy-related genes among different OSRG signature subgroups

Drug response data from the OncoPredict and GDSC databases were predicted using drug responses in TCGA-LUAD dataset. Correlations between IC50 values and risk scores were determined, and discrepancies in IC50 values involving groups with a high- and low-risk score were evaluated. This investigation aimed to evaluate any possible relationships between reaction to treatment and risk score. Patients with LAUD in the high-risk score group in this research exhibited greater sensitivity to docetaxel, ATR kinase inhibitors, WEE1, ERK1, and ERK2 inhibitors, as well as PLK inhibitors, than did the low-risk group. In contrast, Resistance to ROCK inhibitors, Akt1/2/3 inhibitors, BRD4 inhibitors, CDK4/6 inhibitors, insulin receptor inhibitors, and MAPK inhibitors was more probable to develop in the group with a high risk score.The findings showed a substantial positive association involving risk score and IC50 values of the medications: GSK269962A_1192, MK2206_1053, JQ1_2172, Ribociclib_1632, BMS754807_2171, and Doramapimod_042, where IC50 values were substantially higher in the group at high-risk. The IC50 values of the drugs AZD6738_1917, MK1775_1179, SCH772984_1564, ERK_6604_1714, Docetaxel _1007 and BI 2536_1086 exhibited a significant inverse correlation with risk score, and in low-risk group, their IC50 values were markedly greater. These drugs exhibited poor efficacy in low-risk group (Fig. 8A and B).

To find out if tumor risk score can accurately predict the outcome of immunotherapy in LUAD patients, we also performed TIDE correlation analysis utilizing TCGA-LUAD gene expression data. The results revealed that patients who responded well to immunotherapy had lower risk scores, suggesting that this group of patients was far more probable tto react positively to treatment. A model

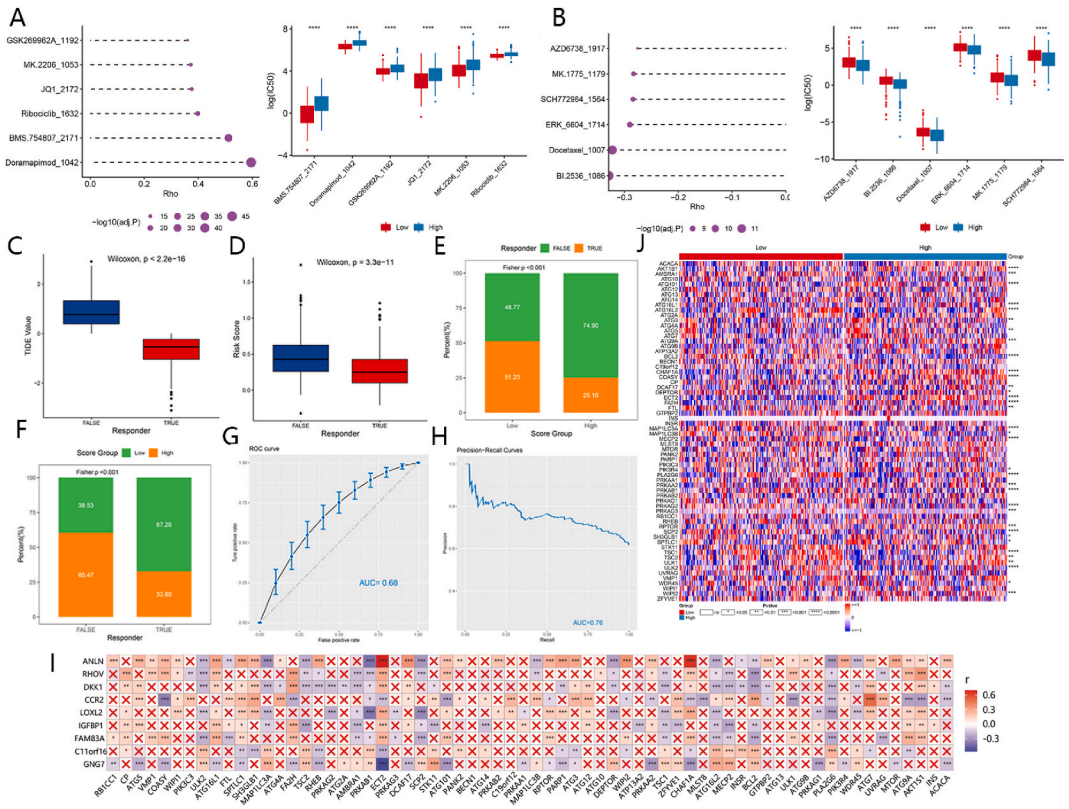

Fig. 8. Analysis of drug response and autophagy-related genes among different signature subgroups. (**A**) Correlation of IC50 values for anticipated medications with risk scores in the training set cohort. (**B**) Differences in IC50 values for anticipated medications between samples in different high and low-risk groups. (**C**) TIDE values in treatment response vs. non-response groups. (**D**) Risk score in the non-response groups vs. treatment response. (**E, F**) The relationship between treatment response in high and low risk categories. (**G, H**) Risk score predicts effect, G is the ROC curve and H is the PR curve. (**I**) Heat map showing the correlation between signature genes and autophagy-related genes. (**J**) Heat map showing autophagy-related gene manifestation in subgroups with low and high risk scores.

using risk score to predict the effect of immunotherapy was proven to be valid, AUC value for the ROC curve was 0.68, and the AUC value for the PR curve was 0.76. Both AUC values were greater than 0.5 (Fig. 8C–H). We next retrieved autophagy-related genes by accessing the PathCards database, to investigate the association between autophagy-related genes and the OSRGs that were utilized to create the tumor risk score. Differences in expression of the nine key oxidative stress genes we screened and autophagy-related genes suggest that the same target genes may exist between our model and autophagy (Fig. 8I). Additionally, we examined the variations in autophagy-associated gene expression levels across risk-score categories. (Fig. 8J). Autophagy-related genes such as *AMBRA1, ATG9A, BCL2, MAP1LC3A,* and *MAP1LC3B* differed significantly in high and low-risk score subgroups.

3.8. Validation of nine prognostic genes for model construction in LUAD cell lines

As verified by qRT-PCR, *ANLN*, *FAM83A*, *RHOV*, and *IGFBP1* were substantially expressed in the majority of LUAD cell lines (Fig. 9A, B, E, F), while *CCR2* and *C11orf16* (Fig. 9G–I) were exhibited by the majority of LUAD cell lines at modest levels. *LOXL2* and *DKK1* showed a trend toward insufficient expression in LUAD cell lines (Fig. 9D–C), while *GNG7* was extremely expressed, which may be related to differences among cell lines (Fig. 9H).

3.9. Verification of DKK1 functions in LUAD cell lines

We selected DKK1 from nine key prognostic genes for functional test validation. We discovered that A549 and H1299 cell growth was decreased by lowering DKK1 expression (Fig. 10A, B, C). In addition, migration assays showed that low DKK1 expression prevented A549 and H1299 cells from migrating (Fig. 10D and E).

4. Discussion

Recent years have seen improvements in the identification and management of LUAD, however, the effectiveness of treatments for

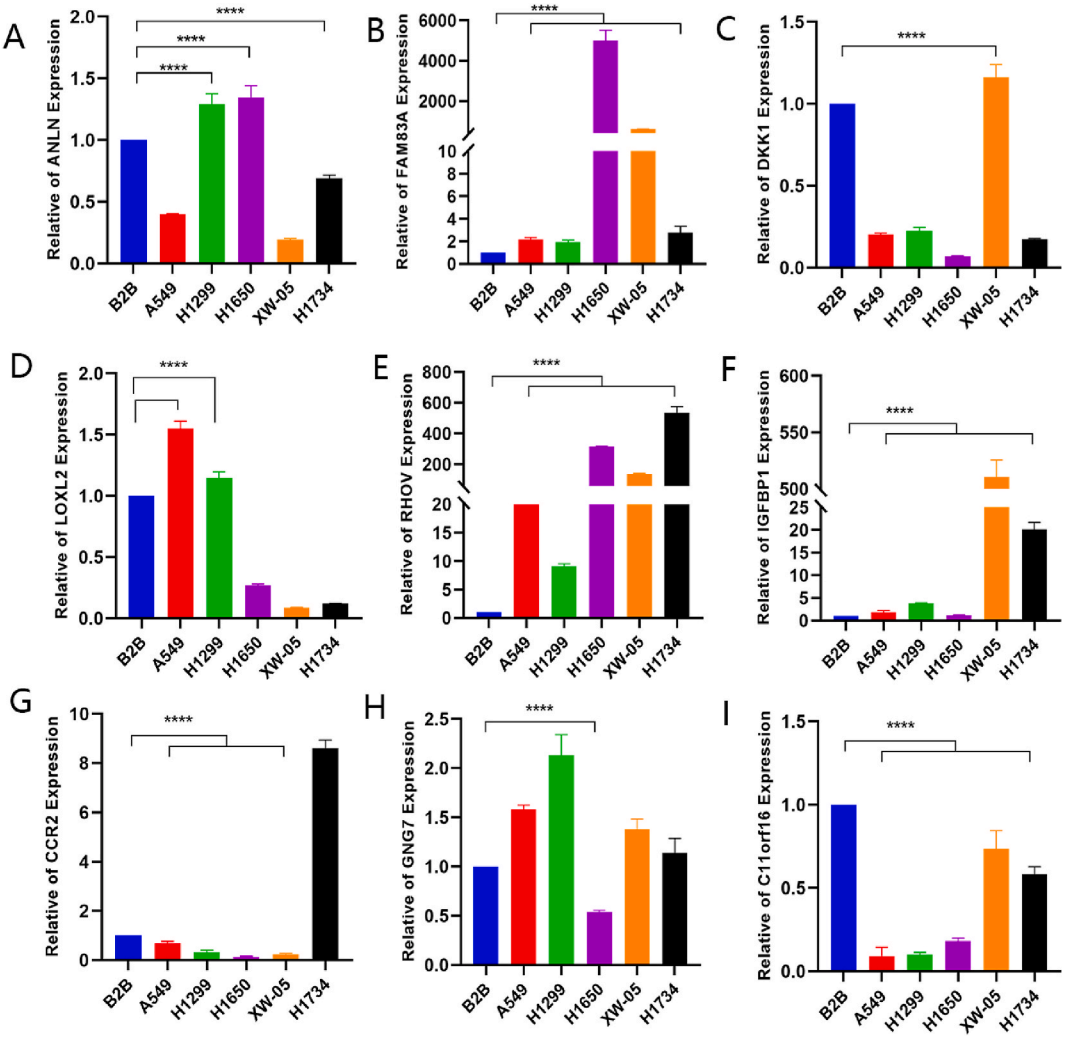

Fig. 9. Validation of nine prognostic genes used for model construction in LUAD cell lines. (**A**) qPCR verified the expression of key gene *ANLN* in LUAD cell lines. (**B**) qPCR verified the expression of key gene *FAM83A* in LUAD cell lines. (**C**) qPCR verified the expression of key gene *DKK1* in LUAD cell lines. (**D**) qPCR verified the expression of key gene *LOXL2* in LUAD cell lines. (**E**) qPCR verified the expression of key gene *RHOV* in LUAD cell lines. (**F**) qPCR verified the expression of key gene *IGFBP1* in LUAD cell lines. (**G**) qPCR verified the expression of key gene *CCR2* in LUAD cell lines. (**H**) qPCR verified the expression of key gene *GNG7* in LUAD cell lines. (**I**) qPCR verified the expression of key gene *C11orf16* in LUAD cell lines. $^{****}p < 0.0001$.

advanced lung cancer remains limited. Five-year survival for LUAD patients is still dismal despite significant advances in combo therapy [16]. Therefore, it is necessary to search for biomarkers that can enhance patient prognosis and provide effective treatment options. For our work, we developed a predictive model founded on OSRGs that may aid physicians in estimating the prognosis of LUAD and potentially selecting appropriate treatment regimens for individual patients. Furthermore, we examined the connection with autophagy-related genes and OSRGs, autophagy or oxidative stress may have cross-links in the relevant pathways, providing new avenues for investigating the treatment of both.

The TCGA database included 436 genes associated with oxidative stress that were differentially expressed. The DEGs were found using a univariate Cox regression analysis, and the optimal range was narrowed using a LASSO regression analysis. Ultimately, it was shown that nine OSRGs—ANLN, FAM83A, DKK1, LOXL2, RHOV, IGFBP1, CCR2, GNG7, and C11orf16—were connected to the outcome of LUAD patients. ANLN, FAM83A, DKK1, LOXL2, RHOV, IGFBP1, CCR2, GNG7, and C11orf16 influence cancer progression in different ways in cancer, and these genes are associated with oxidative stress. Research shows that upregulation of the ANLN gene reduced the efficacy of chemotherapy and immunotherapy in LUAD patients and upregulated the expression of proteins linked to epithelial-mesenchymal transition (EMT)-related proteins [17]. Upregulated FAM83A increases EMT, migratory ability, and cell proliferation in LUAD cell lines [18]. In gastric cancer and head and neck squamous cell carcinoma influence the transformation of epithelium to mesenchyme, and promote resistance to radiotherapy and immunotherapy [19,20]. Through its effects on proliferation, EMT, apoptosis, invasion, and migration, LOXL2 promotes the development and spread of lung cancer [21]. In LUAD, RhoV

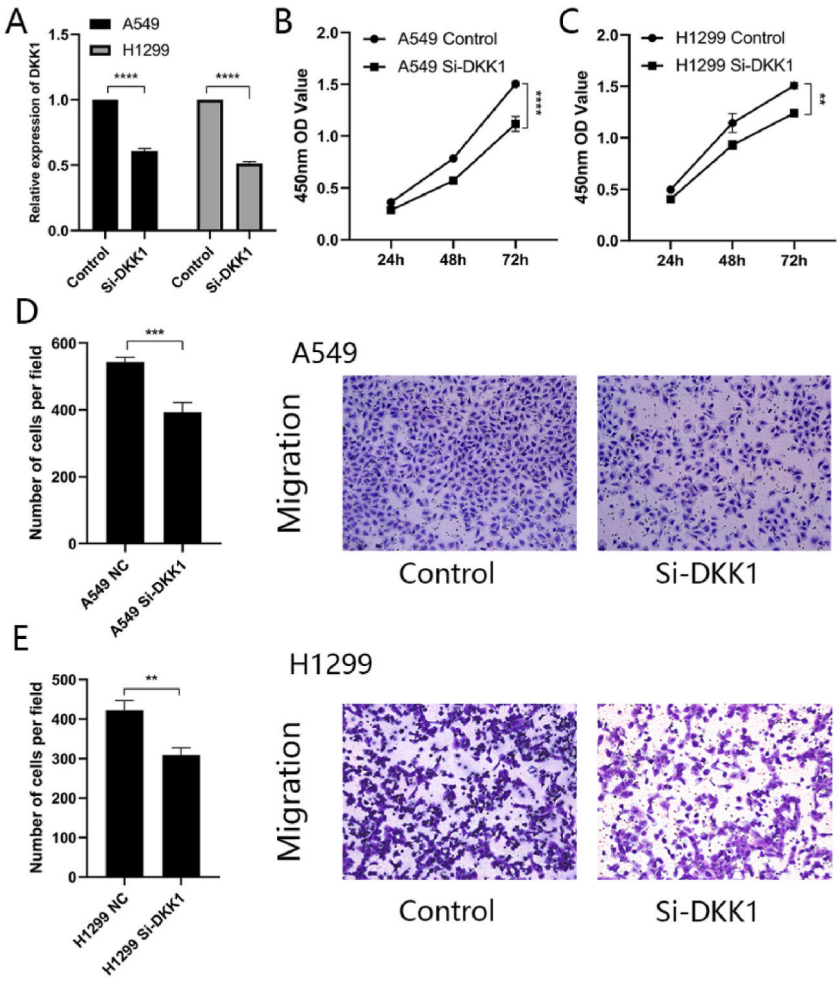

Fig. 10. Verification of DKK1 functions in LUAD cell lines. (**A**) qPCR verified expression after knockdown of DKK1 in A549 and H1299 cell. (**B, C**) Knockdown DKK1 reduced the ability of A549 and H1299 cells to proliferate. (**D, E**) Knockdown DKK1 inhibited the migration function in A549 and H1299 cell.

overexpression accelerates the disease's development and EGFR-TKI resistance [22]. Overexpression of IGFBP1 promotes endocrine therapy resistance in breast cancer [23]. IGFBP1 promotes lung cancer metastasis by enhancing mitochondrial ROS decline [24]. CCL2 stimulates breast cancer cells' growth, survival, and glycolysis [25]. GNG7 is weakly expressed in LUAD and enhances LUAD progression via Hedgehog signaling [26]. The results of the study show that C11orf16 (AAMDC) overexpression may impact outcomes in BC. The nuclear envelope seen in C11orf16 is linked to increased mortality as well as better resistance to statins and responsiveness to FU-based chemotherapies [27]. In conclusion, these nine ros-related genes are involved in pathological oxidative stress during LUAD development and contribute significantly to the onset of cancer. They may therefore be applied to LUAD prognostic prediction.

Since the inception of immunotherapy, clinical standards of care for many tumors have been progressively revised. For individuals with advanced LUAD, immunotherapy is essential for advancing their clinical prognosis [28]. Immune cells linked with tumors are crucial for the growth, metastasis, and recurrence of tumors as well as for the efficacy of immunotherapy [29]. They may be employed as biological markers to forecast a patient's prognosis or the effectiveness of immunotherapeutic treatments. In line with the findings of similar investigations [30], our research model investigated the link throughout the tumor microenvironment and oxidative stress, high-risk group have greater levels of immunosuppression than those in the low-risk group. Furthermore, we discussed the sensitivity to therapeutic agents in both groups of patients. The high-risk score group of LAUD patients exhibited more reactivity to docetaxel, ATR kinase inhibitors, WEE1, ERK1, ERK2, and PLK inhibitors. Conversely, the group with high-risk score had a greater likelihood of developing resistance to ROCK inhibitors, Akt1/2/3 inhibitors, BRD4 inhibitors, CDK4/6 inhibitors, insulin receptor inhibitors, and MAPK inhibitors. Our results demonstrated a correlation between autophagy and oxidative stress genes. Autophagy may be induced and regulated by changes in the redox condition of cells, which cells can exploit to manage redox metabolism under diverse stress conditions [31,32]. For the purpose of laying the groundwork for future studies on the disruption of autophagy and OSRGs, more study on these topics is required. Our study reveals patient sensitivity to anti-tumour drugs, validated by at-risk populations, and a link to autophagy, These findings may help researchers create highly effective therapeutic regimens.

Similar to this study, previous research has been based on expression data for specific genes and involved using LASSO-Cox regression analysis to create an optimal predictive model. Predictive models of oxidative stress genes in lung adenocarcinoma are also discussed in related studies, and similarly, oxidative stress and LUAD development have a strong association [33,34]. In contrast, the efficacy of our prediction model was superior to that of the other studies, with higher AUC values in 1, 3, and 5-year survival ROC curves estimated by the OS features than in the other two studies. Based on our and their research, these genes that are utilized for prognostic model prediction may be used to forecast the prognosis of LUAD, deliver a foundation for LUAD oxidative stress-related research, and provide a new direction for anti-tumour therapy. There are also relevant prognostic models forecast the outlook of LUAD individuals [35–39], and some of the genes are consistent with this study, further demonstrating the role of the key genes we identified in lung adenocarcinoma. In addition, we analysed the correlation between immunotherapy, targeted therapy, and chemotherapy across several risk categories, and we contributed to the prediction of relevant treatments. Similarly, the addition of our study discusses an association between oxidative stress and autophagy. Certain restrictions apply to this investigation. Specifically, the data utilized in our study is derived from pertinent studies involving patients who have had surgical procedures or biopsy examinations, and is sourced from public sources. We need to consider the applicability of this data to patients without surgical specimens. Additionally, some physiologically important genes may be missed while identifying prognostic genes using Cox regression analysis. Furthermore, the limited clinical information and experimental samples in the database may impact the accuracy of our predictive models. More real-world studies may be necessary to confirm the clinical value of our gene signature. It is essential to further research the functioning workings of OSRGs in LUAD further to validate predictive genes through more vitro experiments. Lastly, further validating predictive models in multicenter and large-scale clinical trials is necessary to address these limitations.

5. Conclusion

Our data demonstrate that LUAD is associated with OSRGs and We created a LUAD risk score model via OSRG levels. Considering the links between the model and clinical characteristics, immune infiltration, drug sensitivity, immunotherapy, and autophagy. Patients with LUAD may benefit from therapy that targets OSRGs.

Data availability

The data that support the findings of the present study are openly available in GEO (https://www.ncbi.nlm.nih.gov/geo/) and TCGA (https://portal.gdc.cancer.gov/). Data will be made available on request.

Has data associated with your study been deposited into a publicly available repository? No.

Ethics approval and consent to participate

Not applicable.

Consent for publication

Not applicable.

Funding

The research project 2022Y220 by the Yunnan Provincial Department of Education, the Yunnan Provincial Training Special Funds for High-Level Health Technical Personnel (Nos. L-2018001 and D-2019030), the Yunnan Provincial Training Funds for Middle-Young Academic and Technical Leader Candidate (No. 202005AC160025), and the Yunnan Fundamental Research Projects (Nos. 202001AS070011 and 202201AY070001-221) all provided funding for this study.

CRediT authorship contribution statement

Lan Li: Writing – original draft, Visualization, Validation, Software, Methodology, Investigation, Funding acquisition, Formal analysis, Data curation. **Rujia Qin:** Writing – original draft, Visualization, Software, Methodology, Investigation, Formal analysis. **Xuefeng Wang:** Writing – original draft, Visualization, Software, Resources, Methodology, Investigation, Formal analysis, Data curation. **Ke Cao:** Visualization, Validation, Software, Methodology, Investigation, Formal analysis, Data curation. **Fei Lu:** Visualization, Validation, Software, Methodology, Formal analysis. **Zhengting Chen:** Supervision, Software, Resources, Methodology, Investigation. **Jingyan Gao:** Software, Resources, Methodology, Investigation, Data curation. **Linbo Qiu:** Visualization, Validation, Methodology. **Sisong Shu:** Visualization, Validation, Methodology. **Han Lu:** Visualization, Validation. **Li Chang:** Writing – review & editing, Supervision, Resources, Project administration, Funding acquisition, Data curation, Conceptualization. **Wenhui Li:** Writing – review & editing, Supervision, Resources, Project administration, Funding acquisition, Data curation, Conceptualization.

Declaration of competing interest

The authors declare that they have no known competing financial interests or personal relationships that could have appeared to

influence the work reported in this paper.

Appendix A. Supplementary data

Supplementary data to this article can be found online at https://doi.org/10.1016/j.heliyon.2024.e38306.

References

[1] J. Bar, E. Ofek, I. Barshack, T. Gottfried, O. Zadok, I. Kamer, D. Urban, M. Perelman, A. Onn, Transformation to small cell lung cancer as a mechanism of resistance to immunotherapy in non-small cell lung cancer, Lung Cancer 138 (2019) 109–115, https://doi.org/10.1016/j.lungcan.2019.09.025.

[2] M. Altai, H. Liu, H.Z. Ding, B. Mitran, P.H. Edqvist, V. Tolmachev, A. Orlova, T. Gräslund, Affibody-derived drug conjugates: potent cytotoxic molecules for treatment of HER2 over-expressing tumors, J. Contr. Release 288 (2018) 84–95, https://doi.org/10.1016/j.jconrel.2018.08.040.

[3] D. Planchard, S. Popat, K. Kerr, S. Novello, E.F. Smit, C. Faivre-Finn, T.S. Mok, M. Reck, P.E. Van Schil, M.D. Hellmann, S. Peters, Metastatic non-small cell lung cancer: ESMO Clinical Practice Guidelines for diagnosis, treatment and follow-up, Ann. Oncol. 29 (Suppl 4) (2019) iv192–iv237, https://doi.org/10.1093/annonc/mdy474.

[4] P.N. Lee, B.A. Forey, K.J. Coombs, P.J. Lipowicz, S. Appleton, Time trends in never smokers in the relative frequency of the different histological types of lung cancer, in particular adenocarcinoma, Regul. Toxicol. Pharmacol. 74 (2016) 12–22, https://doi.org/10.1016/j.yrtph.2015.11.016.

[5] I. Dalle-Donne, R. Rossi, R. Colombo, D. Giustarini, A. Milzani, Biomarkers of oxidative damage in human disease, Clin. Chem. 52 (4) (2006) 601–623, https://doi.org/10.1373/clinchem.2005.061408.

[6] A. Agarwal, A. Aponte-Mellado, B.J. Premkumar, A. Shaman, S. Gupta, The effects of oxidative stress on female reproduction: a review, Reprod. Biol. Endocrinol. 10 (2012) 49, https://doi.org/10.1186/1477-7827-10-49.

[7] S. Tangvarasittichai, Oxidative stress, insulin resistance, dyslipidemia and type 2 diabetes mellitus, World J. Diabetes 6 (3) (2015) 456–480, https://doi.org/10.4239/wjd.v6.i3.456.

[8] Z. Wang, Z. Li, Y. Ye, L. Xie, W. Li, Oxidative stress and liver cancer: etiology and therapeutic targets, Oxid. Med. Cell. Longev. 2016 (2016) 7891574 v10.1155/2016/7891574.

[9] J.D. Hayes, A.T. Dinkova-Kostova, K.D. Tew, Oxidative stress in cancer, Cancer Cell 38 (2) (2020) 167–197, https://doi.org/10.1016/j.ccell.2020.06.001.

[10] D.T. Stefanou, M. Kouvela, D. Stellas, K. Voutetakis, O. Papadodima, K. Syrigos, V.L. Souliotis, Oxidative stress and deregulated DNA damage response network in lung cancer patients, Biomedicines 10 (6) (2022) 1248, https://doi.org/10.3390/biomedicines10061248.

[11] Z. Wang, Z. Li, Y. Ye, L. Xie, W. Li, Oxidative stress and liver cancer: etiology and therapeutic targets, Oxid. Med. Cell. Longev. 2016 (2016) 7891574 v10.1155/2016/7891574.

[12] N.S. Brown, R. Bicknell, Hypoxia and oxidative stress in breast cancer. oxidative stress: its effects on the growth, metastatic potential and response to therapy of breast cancer, Breast Cancer Res. 3 (5) (2001) 323–327, https://doi.org/10.1186/bcr315.

[13] J.D. Hayes, A.T. Dinkova-Kostova, K.D. Tew, Oxidative stress in cancer, Cancer Cell 38 (2) (2020) 167–197, https://doi.org/10.1016/j.ccell.2020.06.001.

[14] B. Kumar, S. Koul, L. Khandrika, R.B. Meacham, H.K. Koul, Oxidative stress is inherent in prostate cancer cells and is required for aggressive phenotype, Cancer Res. 68 (6) (2008) 1777–1785, https://doi.org/10.1158/0008-5472.CAN-07-5259.

[15] R. Visconti, D. Grieco, New insights on oxidative stress in cancer, Curr. Opin. Drug Discov. Dev 12 (2) (2009) 240–245.

[16] Z. Chen, C.M. Fillmore, P.S. Hammerman, C.F. Kim, K.K. Wong, Non-small-cell lung cancers: a heterogeneous set of diseases, Nat. Rev. Cancer 14 (8) (2014) 535–546, https://doi.org/10.1038/nrc3775.

[17] Q. Cao, H. Wang, J. Zhu, et al., lncRNA CYTOR promotes lung adenocarcinoma gemcitabine resistance and epithelial-mesenchymal transition by sponging miR-125a-5p and upregulating ANLN and RRM2, ACTA BIOCH BIOPH SIN 56 (2) (2024) 210–222, https://doi.org/10.3724/abbs.2023287.

[18] C. Zhao, X. Li, R. Zhang, et al., Sense and anti-sense: role of FAM83A and FAM83A-AS1 in Wnt, EGFR, PI3K, EMT pathways and tumor progression, Biomed. Pharmacother. 173 (2024) 116372, https://doi.org/10.1016/j.biopha.2024.116372.

[19] X. Ye, J. Liu, R. Quan, et al., DKK1 affects survival of patients with head and neck squamous cell carcinoma by inducing resistance to radiotherapy and immunotherapy, Radiother. Oncol. 181 (2023) 109485, https://doi.org/10.1016/j.radonc.2023.109485.

[20] J. Li, Y. Zhang, F. Ye, et al., DKK1 promotes epithelial-mesenchymal transition and cisplatin resistance in gastric cancer via activation of the PI3K/AKT pathway, Cancers 15 (19) (2023), https://doi.org/10.3390/cancers15194756.

[21] L. Fan, W. Jiang, C. Chen, et al., CEBPA facilitates LOXL2 and LOXL3 transcription to promote BCL-2 stability and thus enhances the growth and metastasis of lung carcinoma cells in vitro, Exp. Cell Res. 435 (2) (2024) 113937, https://doi.org/10.1016/j.yexcr.2024.113937.

[22] H. Chen, R. Xia, L. Jiang, et al., Overexpression of RhoV promotes the progression and EGFR-TKI resistance of lung adenocarcinoma, Front. Oncol. 11 (2021) 619013, https://doi.org/10.3389/fonc.2021.619013.

[23] J. Kieltyka, Y. Zheng, A. Hobbs, et al., Overexpression of insulin-like growth factor binding protein 1 (IGFBP1) generates tamoxifen resistance in breast cancer cells, FASEB J 32 (S1) (2018), https://doi.org/10.1096/fasebj.2018.32.1_supplement.804.57.

[24] G. Cai, Y. Qi, P. Wei, et al., IGFBP1 sustains cell survival during spatially-confined migration and promotes tumor metastasis, Adv. Sci. 10 (21) (2023-07-01) e2206540, https://doi.org/10.1002/advs.202206540.

[25] D.S. Acevedo, W.B. Fang, V. Rao, Regulation of growth, invasion and metabolism of breast ductal carcinoma through CCL2/CCR2 signaling interactions with MET receptor tyrosine kinases, Neoplasia 28 (2022) 100791, https://doi.org/10.1016/j.neo.2022.100791.

[26] X. Zhao, X.C. Zhang, K. Zang, MicroRNA miR-19b-3p mediated G protein γ subunit 7 (GNG7) loss contributes lung adenocarcinoma progression through activating Hedgehog signaling, Bioengineered 12 (1) (2021) 7849–7858, https://doi.org/10.1080/21655979.2021.1976896.

[27] I. Weerasena, L. Spalding, B. Dessauvagie, et al., Abstract P5-05-03: adipocyte associated methionine domain containing (AAMDC): a nuclear envelope protein with predictive and prognostic potential in luminal breast cancer, Cancer Res. 82 (4_Supplement) (2022), https://doi.org/10.1158/1538-7445.sabcs21-p5-05-03. P5-05-03-P5-05-03.

[28] H. Borghaei, L. Paz-Ares, L. Horn, D.R. Spigel, M. Steins, N.E. Ready, L.Q. Chow, E.E. Vokes, E. Felip, E. Holgado, Nivolumab versus docetaxel in advanced nonsquamous non-small-cell lung cancer, N. Engl. J. Med. 373 (2015) 1627–1639, https://doi.org/10.1056/NEJMoa1507643.

[29] K.A. Schalper, J. Brown, D. Carvajal-Hausdorf, J. McLaughlin, V. Velcheti, K.N. Syrigos, et al., Objective measurement and clinical significance of TILs in non-small cell lung cancer, J Natl Cancer Inst 107 (2015), https://doi.org/10.1093/jnci/dju435.

[30] M.D. Hellmann, T. Nathanson, H. Rizvi, B.C. Creelan, F. Sanchez-Vega, A. Ahuja, et al., Genomic features of response to combination immunotherapy in patients with advanced non-small-cell lung cancer, Cancer Cell 33 (5) (2018) 843–852. e4, https://doi.org/10.1016/j.ccell.2018.03.018.

[31] M. Cordani, M. Sanchez-Alvarez, R. Strippoli, A.V. Bazhin, M. Donadelli, Sestrins at the interface of ROS control and autophagy regulation in health and disease, Oxid. Med. Cell. Longev. 2019 (2019) 1283075, https://doi.org/10.1155/2019/1283075.

[32] V. Roca-Agujetas, C. de Dios, L. Leston, M. Mari, A. Morales, A. Colell, Recent insights into the mitochondrial role in autophagy and its regulation by oxidative stress, Oxid. Med. Cell. Longev. 2019 (2019) 3809308, https://doi.org/10.1155/2019/3809308.

[33] Y. Zhu, Q. Tang, W. Cao, et al., Identification of a novel oxidative stress-related prognostic model in lung adenocarcinoma, Front. Pharmacol. 13 (2022) 1030062, https://doi.org/10.3389/fphar.2022.1030062.

[34] H. Peng, X. Li, Y. Luan, et al., A novel prognostic model related to oxidative stress for treatment prediction in lung adenocarcinoma, Front. Oncol. 13 (2023) 1078697, https://doi.org/10.3389/fonc.2023.1078697.
[35] Q. Li, X.L. Liu, N. Jiang, et al., A new prognostic model for RHOV, ABCC2, and CYP4B1 to predict the prognosis and association with immune infiltration of lung adenocarcinoma, J. Thorac. Dis. 15 (4) (2023) 1919–1934, https://doi.org/10.21037/jtd-23-265.
[36] Q. Zhang, M. Zhao, S. Lin, et al., Prediction of prognosis and immunotherapy response in lung adenocarcinoma based on CD79A, DKK1 and VEGFC, Heliyon 9 (8) (2023) e18503, https://doi.org/10.1016/j.heliyon.2023.e18503.
[37] D. Zhang, Y. Zhao, Identification of natural killer cell associated subtyping and gene signature to predict prognosis and drug sensitivity of lung adenocarcinoma, Front. Genet. 14 (2023) 1156230, https://doi.org/10.3389/fgene.2023.1156230.
[38] G. Wu, Y. Wang, Y. Wan, Establishing an 8-gene immune prognostic model based on TP53 status for lung adenocarcinoma, J. Clin. Lab. Anal. 36 (7) (2022) e24538, https://doi.org/10.1002/jcla.24538.
[39] W. Ma, J. Liang, J. Liu, et al., Establishment and validation of an eight-gene metabolic-related prognostic signature model for lung adenocarcinoma, Aging (Albany NY) 13 (6) (2021) 8688–8705, https://doi.org/10.18632/aging.202681.